Franz W. Leberl [1], Kelly Maurice [2], John K. Thomas [3] and Michel Millot [4]

Automated radar image matching experiment

Stereo-parallax measurements for digital elevation extraction, matching for change detection, and creation of stacks of multi-temporal or multi-incidence angle images ("cubes") of co-registered images all can be supported by automation via computerized image correlation. Precision parallax measurements are traditionally made by an experienced stereo-operator. Automated methods have been investigated, but have not found wide acceptance.

Radar mapping, for example in NASA's Magellan mission to planet Venus, has a requirement to develop Digital Elevation Models (DEM) from stereo radar images, and to match multiple coverages from sequential image acquisition cycles. We report on an experiment to assess the quality of machine-matches for stereo-parallax detection in radar images, and find that there are often ±2 pixel differences between the experienced stereo-operator and the best image-matching method, based on a normalized cross-correlation measure. When comparing this to SPOT-images and to scanned aerial photography, we note that errors of machine matching are typically smaller in those images than in radar images, with SPOT data producing automated matches with subpixel differences to manual matches.

1. Introduction

In order to assess the quality and computational cost of computerized stereo image matching, we performed a set of experiments in support of radar mapping studies. We are motivated by the plan to develop a large number of image matches for about 1800 radar image pairs of planet Venus acquired during the nominal Magellan mission of NASA from 15 September 1990 to 16 May 1991, and during the extension of that mission. Each image pair covers 25 km × 20,000 km or 350 × 250,000 pixels, reaching nearly from pole to pole. With a spacing of the matches at five pixels this would result in three million matches per image pair, and up to five billion matches in total. If done manually at a rate of 3 s per point, this would take 2000 man-years.

The same concerns apply to satellite radar images of the Earth, for example with Canada's Radarsat, Europe's E-ERS-1 or Japan's J-ERS-1, or with other imaging sensors. Unless parallax measurements are made automatically, rapidly and without blunders, a global DEM is not feasible. It is thus of interest to develop experiences with matching of radar images.

There is only little work reported in the radar literature, except on data from the Space Shuttle SIR-B experiment (e.g. Ramapriyan et al., 1986; Simard et al., 1986; Fernin and Nasr, 1990). Some work has been reported in the area of registration of a radar image with a simulated data set for ground control detection (Guindon and Maruyama, 1986; Guindon, 1987).

While stereo matching is a lively research topic with non-radar images, our study aims at identifying the robustness and accuracy of machine-matching two radar images, using current and customary matching algorithms. We abstain from the identification of new and previously unknown methods of matching.

Fig. 1 presents a typical stereo-pair of radar images taken by the Magellan spacecraft during a short one-day stereo-experiment in July 1991. This indicates that slopes facing the radar antenna are compressed, or foreshortened, into rather narrow image regions. At slope angles of 25° one may well find a manifestation in the radar image of a slope in a mere 2 pixels or 150 m, even though the terrain features extend over several kilometers (Fig. 2).

---

[1] VEXCEL Corporation, Boulder, Colo., USA. Currently also at: Graz University of Technology, A-8010 Graz, Austria.

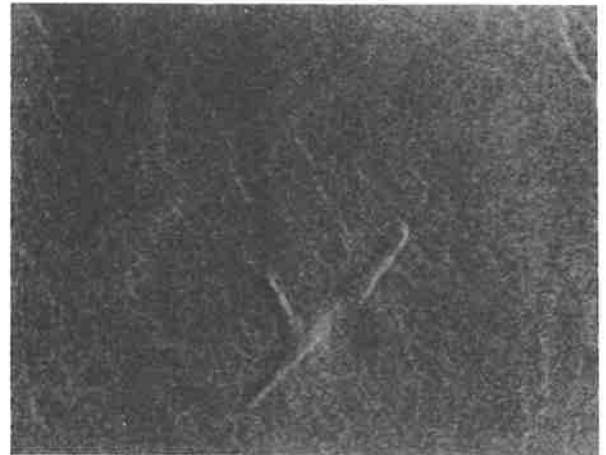[2] VEXCEL Corporation, Boulder, Colo., USA.

[3] VEXCEL Corporation, Boulder, Colo., USA. Currently also at: Electrical Engineering Department, University of Colorado, Boulder, Colo., USA.

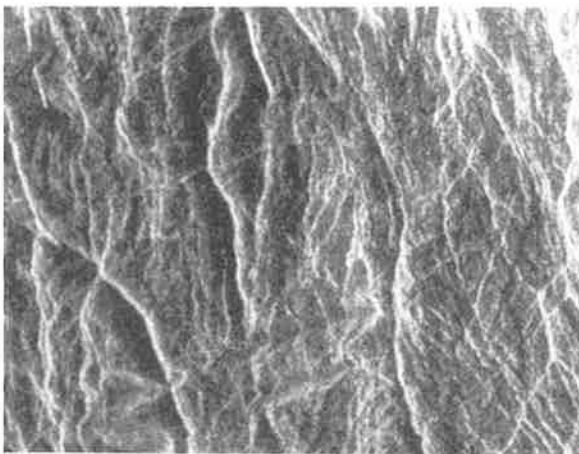[4] VEXCEL Corporation, Boulder, Colo., USA. Present address: 110 Rue Lavoisier, F-78140 Velizy, France.
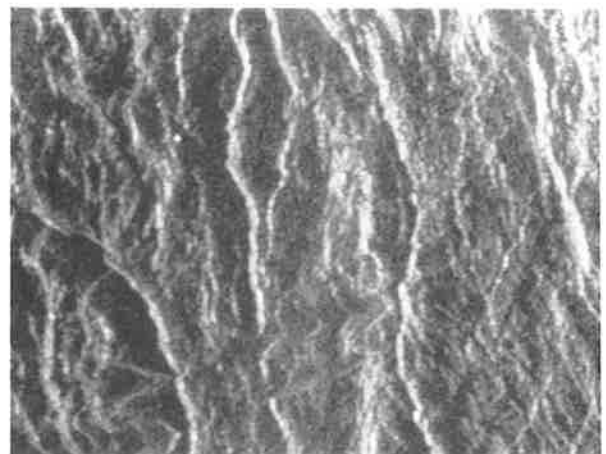
N↑

Figure 1. Example of Magellan radar images (36 km wide × 30 km long) at 8°S, 75°E for two different radar look angles off-nadir and for two types of terrain. (a) Cycle 1 at 40° off-nadir, looking east (smooth terrain). (b) Cycle 2 at 21° off-nadir, looking east (smooth terrain). (c) Cycle 1 at 40° off-nadir, looking east (rough terrain). (d) Cycle 2 at 21° off-nadir, looking east (rough terrain). Note that certain terrain shapes are compressed in these east-looking images.

This is the reason that image measurements of parallaxes must be obtained both near the base as well as near the top of the slope, resulting in a requirement for rather densely spaced match points at an interval of perhaps 5 pixels.

We report here on the assessment of stereo-matching accuracy in a comparison between an experienced human stereo-operator and five often-used image-matching algorithms. These algorithms were applied to Magellan stereo radar test data. To develop an understanding for the technology, we also applied the methods to other sensors, as summarized in Table 1. The human operator put a stereo measuring mark on the ground to serve: (a) as a reference match, and (b) as a "predictor" for the automated matches.

The automated methods were applied to the window around the points observed by the oper-

Table 1

Test data set for the stereo-matching experiment

Radar images	Pixel size (m)	Look-angle off-nadir θ' (°)	Look-angle off-nadir θ'' (°)	Intersection angle $\Delta\theta$ (°)	Typical stereo parallax for terrain elevation $h = 100$ m	Comments
Magellan radar, Set 1	75	40	21	19	140 m	2°S, 75°E
Magellan radar, Set 2	75	25	14	11	187 m	39°S, 79°E
Magellan radar, Set 3	75	15	11	4	141 m	59°S, 86°E
Aircraft radar	6	73	55	18	39 m	Brazeau, Canada
SPOT stereo images	20	2	27	25	47 m	Boulder, Colorado

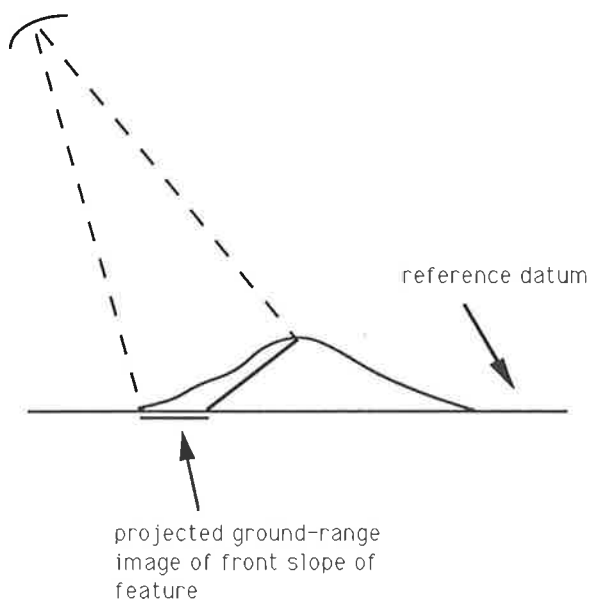|	Pixel size (m)	Flying height (m)	Photo scale	Base-to-height ratio	Stereo parallax for terrain $h = 100$ m	
Digitized National Aerial Photography Program (NAPP)	2	6000	1 : 40,000	0.6	60 m	Boulder, Colorado

Figure 2. Compression of terrain sloping towards the antenna is denoted as "foreshortening" in radar images.

ator. Any differences between the match points found by the operator and by machine were recorded and are reported in this paper.

We found that automated matching in radar images consistently produced matches with a mean offset of 0.5 to 1.5 pixels from the human's measurement, and with a standard deviation often in excess of ±2 pixels. We find that these errors are smaller if SPOT images or digitized aerial photographs are used.

2. Matching algorithms

2.1. Overall matching strategies

Image matching needs to be accomplished in an established sequence of events as illustrated in Fig. 3. A candidate match area needs to be identified in a "prediction step", and a specific match-method is applied. This may lead to the need of refining a match, say to a sub-pixel accuracy. Finally, each match must be examined and accepted or
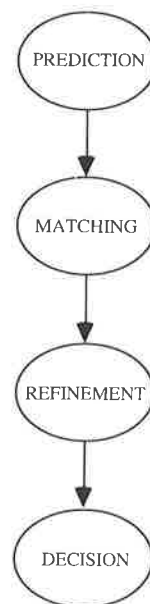

Figure 3. Overall sequence of steps in image-matching methods.

rejected. Many matching procedures operate iteratively, starting at a coarse geometric resolution and refining the result by using finer resolutions (Li, 1991). In essence they work on resolution pyramids and are denoted as "hierarchical" methods. Or they use coarse matches to remove geometric disparities between images in a process called iterative orthorectification (IOR, Norvelle, 1992b).

The actual matching function is the often-discussed core element of a system, but the success of any system depends on the implementation of all steps of the process, not just the core matching method.

2.2. Method description

An enormous body of work exists on image matching. We selected five methods for analysis that are all intensity-based. Radar images do not promise clear edge information, and therefore edge- or feature-based methods were not considered. All matching techniques operate on a reference and search window of image gray values, with x denoting the $M \times M$ array of gray values in the reference, and y the gray values in the search window of dimension $N \times N$ where $N > M$ ($S =$
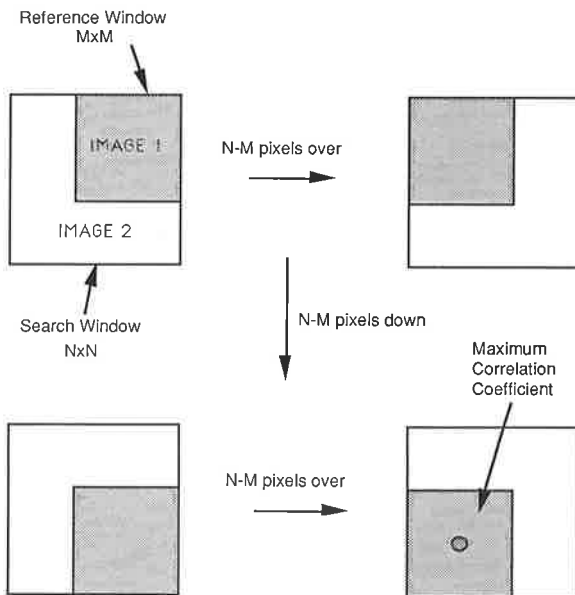

Figure 4. For each position of the search window, a match value is computed. A match is accomplished if the match value at a certain position of the search window has a local maximum when compared with match values at all other positions of the search window.

$N - M$). The search window is moved over the reference, and a match value is computed for each of the $(S + 1) \times (S + 1)$ positions. A best match is obtained by sorting through the match values (see Fig. 4).

2.2.1. Use of normalized correlation (CORREL)

This is often considered to be the most accurate matching method, but at the expense of computing effort. It has been widely discussed, from the early days of image processing, and many computational implementations have been proposed, for example by Anuta (1970). In the current experiment we use:

$$
C = \max_{1 \le i,j \le (N-M+1)}^{r_{i,j}} = \frac{E[(x - \overline{x})(y - \overline{y})]}{\sqrt{E[(x - \overline{x})^2]E[(y - \overline{y})^2]}}
$$
$$
= \frac{\sigma_{xy}}{\sigma_x \sigma_y} = \frac{\left(\sum_{k,l=1}^{M} x_{k,l} y_{i+k,j+l}\right) / M}{\sigma_x \sigma_y}
$$

where:

$$
\sigma_x^2 = \left[\sum_{k,l=1}^{M} (x_{k,l})^2\right] - (M\overline{x})^2
$$

and:

$$
\sigma_y^2 = \left[\sum_{k,l=1}^{M} (y_{i+k,j+l})^2\right] - (M\overline{y})^2
$$

Here $r_{i,j}$ is the correlation coefficient at location i, j in the search window, $x_{k,l}$, $y_{i+k,j+l}$ are the gray values in a reference (master) and search (slave) window and $\overline{x}$, $\overline{y}$ are the means of the gray values in each reference and search window overlap. $E[\ldots]$ is the "expected value". The match point is found as the local maximum of r as r is computed for various positions of the search window on the reference window. This method is preferred if computational cost is not an issue (Crombie and Bosch, 1986). It tends to be slightly more accurate than MNAD below (Svedlow et al., 1978).

2.2.2. Sum of mean normalized absolute differences (MNAD)

This method is similar to normalized correlations in terms of match performance, but requires less computations. One searches for the minimum value of s:

$$
s = E[|(x - \overline{x}) - (y - \overline{y})|]
$$

With radar images, a variant on this approach was used in the SIR-B Space Shuttle experiment by Ramapriyan et al. (1986).

2.2.3. Sum of mean normalized squared differences (SQUARE)

This method implements a least-squares fit that minimizes the squares of the gray-level differences between images (Rosenholm, 1987):

$$s = E\left[(x - \overline{x}) - (y - \overline{y})\right]^2$$

2.2.4. Stochastic sign change (SSC)

This method represents an estimator that uses the integer set criterion of sign changes in subtraction image sequence values. It relies (Herbin et al., 1989) on the presence of noise in the imagery. The implemented version of this algorithm removes the mean from each window intensity to account for a potential offset between the images. It should be noted that the differences are scanned first along the columns.

2.2.5. Outlier minimal number estimator (OMNE)

Also an integer criterion method, similar to SSC, the OMNE is a membership set estimator that utilizes an uncertainty interval for each pixel (Herbin et al., 1989). This method works well for dissimilar images. This method requires an interval parameter.

2.3. Discussion

Just like in interpolation algorithms, image-matching methods exist in great numbers. Each technique is the result of a specific requirement and may be optimal for a narrow set of constraints. These may be the need for computational speed, robustness against image noise, absence of edges, etc.

3. Test data

Matching results may vary with specific imaging parameters. To develop an understanding of the relationships between accuracy and imaging parameters, data sets are required that use images taken under different configurations. Therefore, we rely on various images as listed in Table 1. The three Magellan stereo-pairs are shown in Figs. 1, 5 and 6. They differ in look-angle geometry. Magellan's orbit is elliptical and the radar illumination therefore

needs to change from 42° at periapsis to 11° near the pole (Leberl et al., 1992). The stereo partner is created with look angles of 21° at periapsis and 8° near the pole.

The effect of radar resolution is studied by using aircraft data. We employ a stereo-pair produced by Intera Ltd. with its STAR-1 synthetic aperture radar (Fig. 7). We aim at defining errors of machine-matching as they relate to the ability of an experienced human operator. Since we want to express errors in a dimensionless way, we report them in "pixels". To compare radar to conventional images, we apply the experimental set-up to non-radar images as well, namely SPOT images (Fig. 8) and digitized aerial photography over a region in Colorado with both mountains and flat areas (Fig. 9).

The analysis will separate the results into those for flat and mountainous areas. The sub-areas for these two classes of terrain are shown in the respective figures.

4. Experiment set-up

Fig. 10 explains the experiment. A human operator manually determines the best match between two images. Several hundred matches are set up for each image pair, and for each region selected for study from each pair. These image coordinates represent a file of known match points x'_o, y'_o, x''_o, y''_o in the left (') and right images ("').

The "known" match points are now used as a "prediction" for an automated matching algorithm. A reference and a search window with $M \times M$ and $N \times N$ pixels are selected around the predicted pixel locations. The search window is moved into $(N - M + 1) \times (N - M + 1)$ positions and a correlation value is computed in each position. A "best" correlation match is defined and recorded as x'_o, y'_o, x'', y''.

The manually observed and automatically computed positions are compared as follows:

$$\Delta x = x'' - x''_o$$

$$\Delta y = y'' - y''_o$$

with Δx, Δy considered to be "errors" of the matching process. These are subject to an error analysis. For each image segment one will obtain several hundred Δx, Δy values.
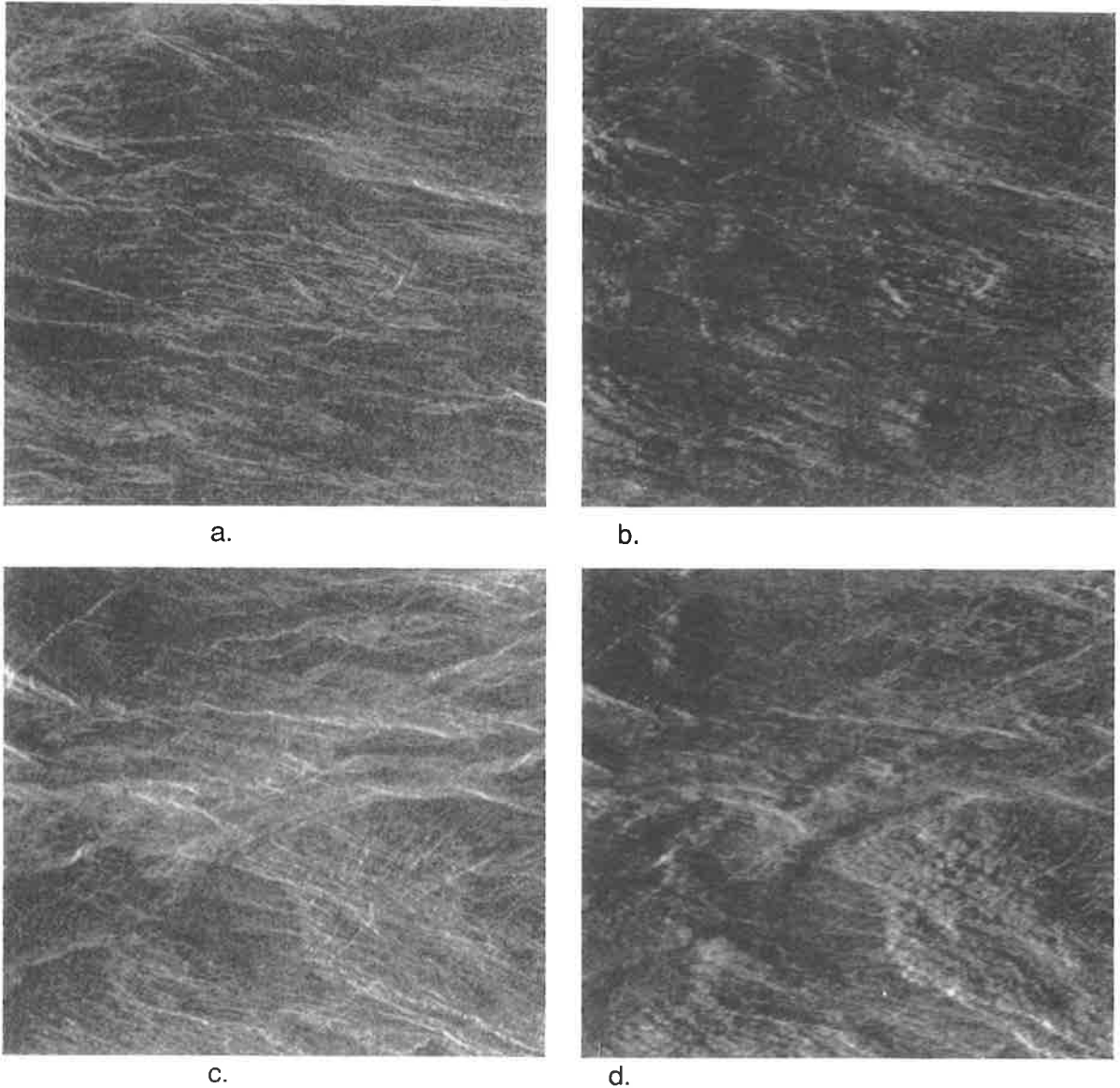
N↑

Figure 5. Magellan stereo image pair (53 km wide × 53 km long) at 39°S 79°E with look-angle geometry of $\theta' = 25°$, $\theta'' = 14°$, $\Delta\theta = 11°$. (a) Cycle 1 (smooth); (b) cycle 2 (smooth); (c) cycle 1 (rough); (d) cycle 2 (rough).

These will be further dependent on specific choices in the matching method and selection of parameters within each method. Of particular interest is the size of the search window, N, and the number of positions over which the maximum match value is determined, $[(N - M + 1)(N - M + 1)]$.

5. Results and discussion

5.1. Accuracy variations in different sensors and terrain types

Table 2 presents a summary of the mean and standard deviation of the error values in the radar
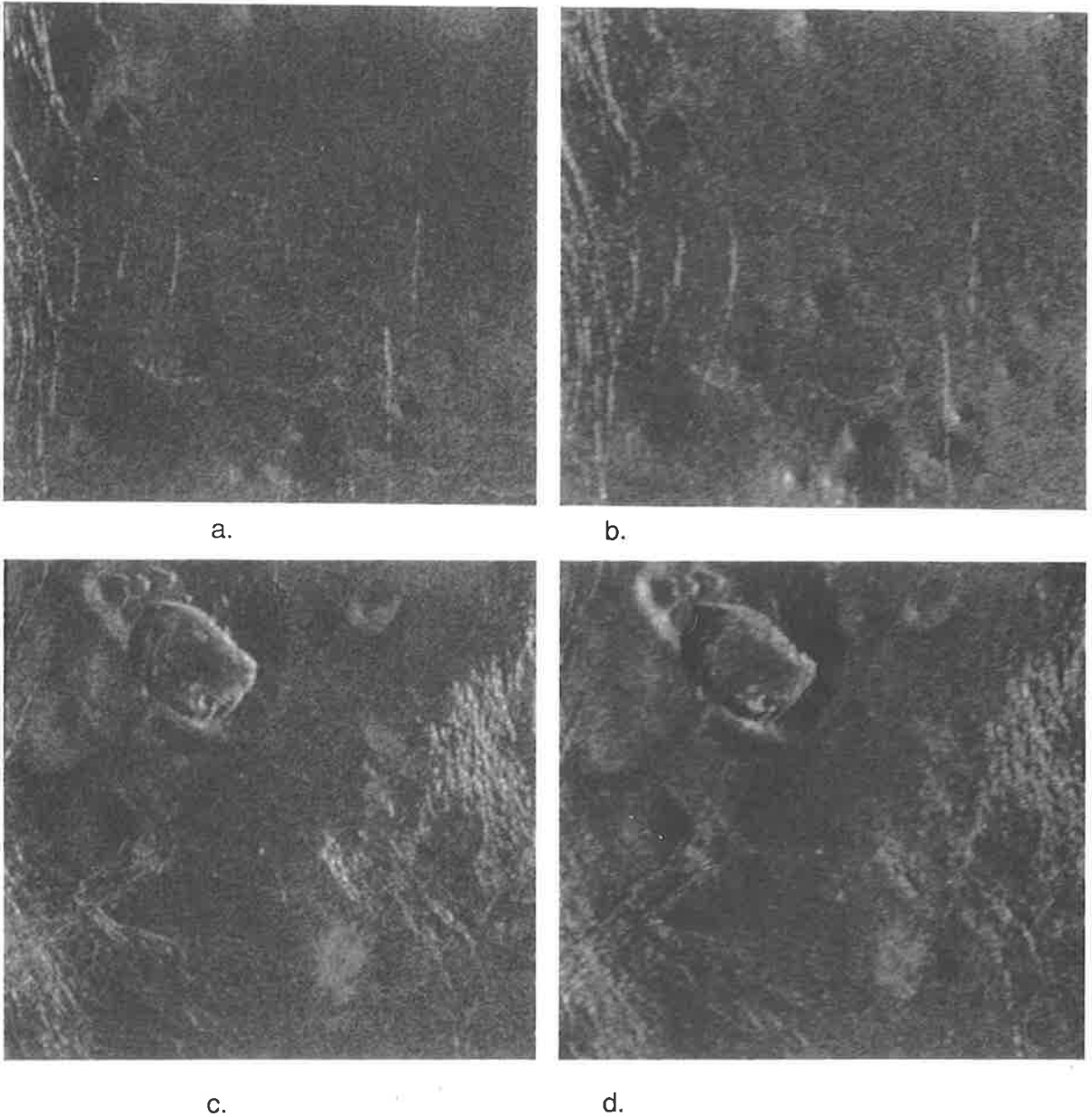
N↑

a.

b.

c.

d.

Figure 6. Magellan stereo image pair (53 km wide × 53 km long) at 59°S 86°E with look-angle geometry of $\theta' = 15°$, $\theta'' = 11°$, $\Delta\theta = 4°$. (a) Cycle 1 (smooth); (b) cycle 2 (smooth); (c) cycle 1 (rough); (d) cycle 2 (rough).

range direction, which are the relevant errors for elevation computation.

$$\Delta x_{mean} = \frac{\sum_{i=1}^{K} \Delta x_i}{K}$$

$$\sigma_{\Delta x} = \sqrt{\frac{\sum_{i=1}^{K}(\Delta x_i - \Delta x_{mean})^2}{K-1}}$$
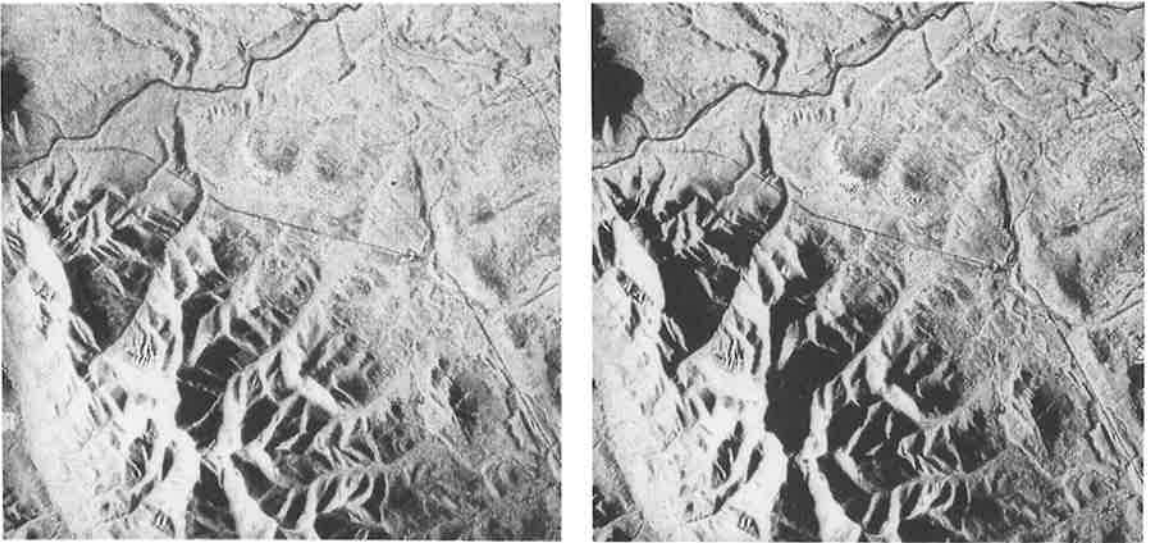
K is the number of points observed manually. The

N↑

Figure 7. Aircraft radar image pair with 6 m pixels at look angles off-nadir of $71.5° < \theta' < 75.3°$, $50.5° < \theta'' < 63°$, with intersection angles of $\Delta\theta = 21°$ at near range and $\Delta\theta = 12°$ at far range. The area is roughly 16 km^2. (Courtesy Intera Technologies Ltd.)
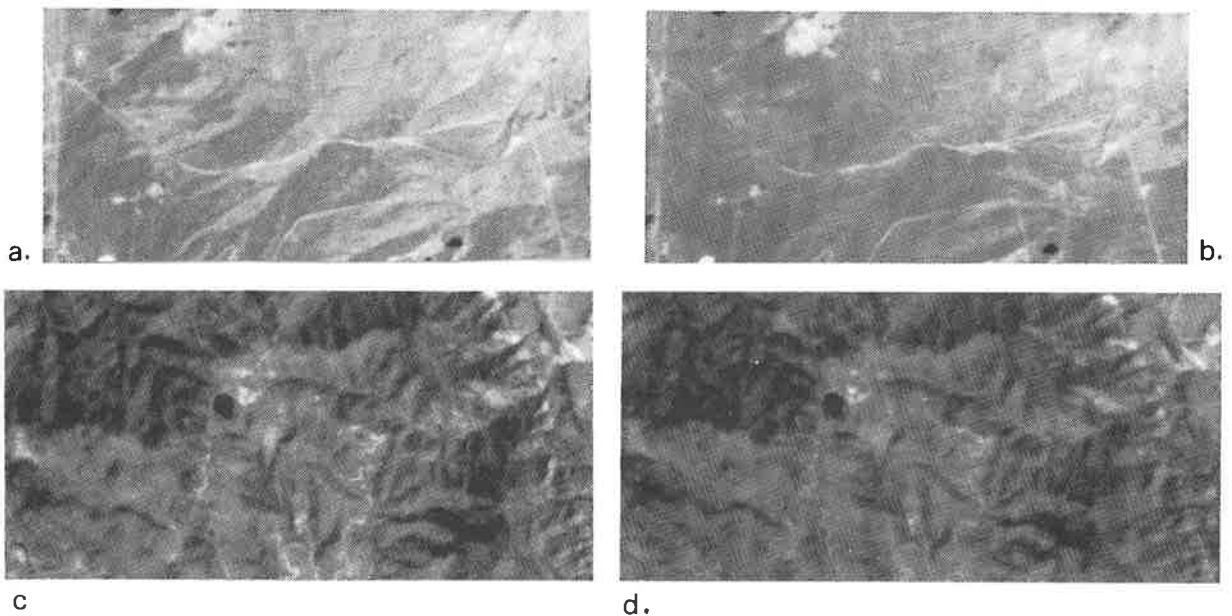
N↑

Figure 8. SPOT image pairs (copyright CNES 1992) with pixels at 20 m over Boulder, Colorado (see Table 1). (a) 2° off-vertical (smooth) (7.2 km wide × 3.9 km long). (b) 27° off-vertical (smooth) (7.2 km wide × 3.9 km long). (c) 2° off-vertical (rough) (7.9 km wide × 4.5 km long). (d) 27° off-vertical (rough) (7.9 km wide × 4.5 km long).
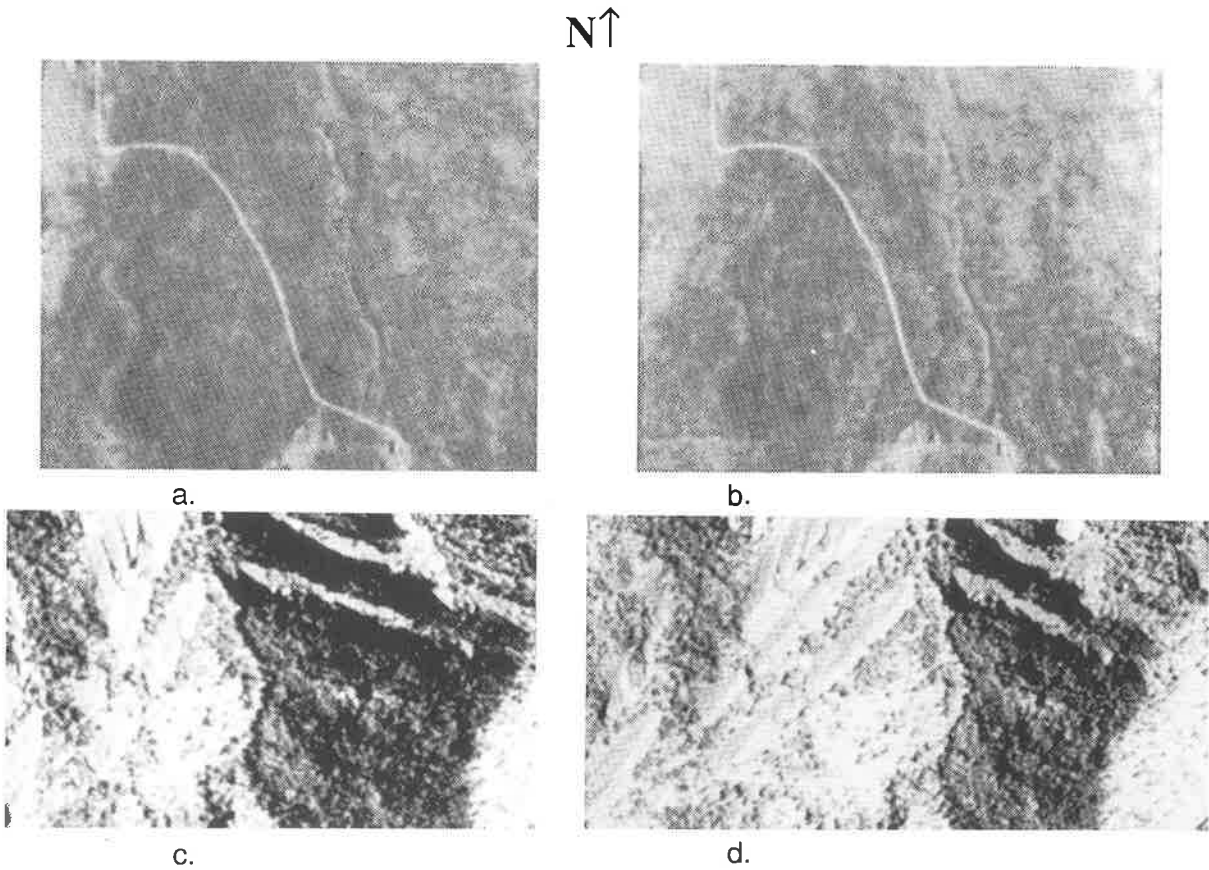
Figure 9. Digitized aerial photography over Boulder, Colorado, with base-to-height ratio of 0.6 (see Table 1): (a), (b) smooth terrain (640 m wide × 570 m long); (c), (d) rough terrain (700 m wide × 450 m long).

Table 2

Machine match versus manual match in range direction (in x), expressed in pixels, using normalized correlation coefficient

Area (Figure)	Intersection		Number of points	Window size M	Smooth		% "Bad" (>1 pixel)	Rugged		%"Bad"
					mean	σ		mean	σ	
1	8°S	19°	340 (smooth)	10	0.7	2.9	93	0.7	2.3	91
			330 (rugged)	20	0.8	2.6	86	0.6	1.8	84
				40	0.8	2.2	76	0.5	1.6	85
5	39°S	11°	225 (smooth)	10	0.7	2.9	87	0.6	2.8	86
			222 (rugged)	20	0.4	2.3	71	0.8	2.3	69
				40	0.6	1.5	50	0.5	1.6	61
6	59°S	4°	225 (smooth)	10	0.1	2.8	88	0.3	2.7	82
			225 (rugged)	20	0.3	2.5	83	0.4	2.3	72
				40	0.0	1.9	75	0.0	1.8	53
7	Intera Star-1	18°	800 (varied terrain)	10	−0.4	1.9	48	−	−	--
				20	−0.6	1.1	26	−	−	−
				40	−0.5	1.0	12	−	−	−
8	SPOT	25°	350 (smooth)	10	0.3	1.1	17	0.2	0.8	17
			432 (rugged)	20	0.3	0.7	7	0.2	0.7	18
				40	0.3	0.5	5	0.4	1.1	33
9	NHAP	33°	440 (smooth)	10	0.3	1.6	40	0.2	1.9	59
			367 (rugged)	20	0.4	0.6	13	0.2	2.2	68
				40	0.5	0.4	9	0.3	2.8	78

A match point is classified as "bad" if it differs by more than one pixel from the match defined by the experienced stereo operator.
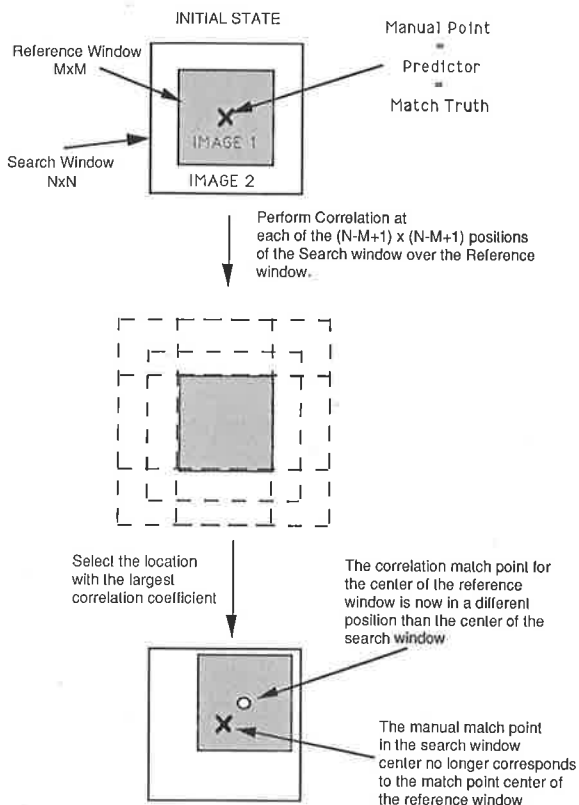
Figure 10. Definition of the matching experiment.

values of M are chosen to be fairly large when compared to work done with photography, and are at 10, 20 and 40 pixels; only the normalized correlation coefficient is used for this table. In this study, by fixing S to be 10, the maximum discrepancy allowed between operator and machine is ± 5 pixels. We selected values of M that are large because we were concerned about the effect of speckle noise and of illumination differences.

We found that the Magellan data mislead automated matching into a match point which deviates by about ± 2 pixels from the manually obtained value. This error remains about the same, irrespective of the look angles off-nadir and of the look-angle disparities. It is to be noted that the human observer is very consistent and will point to a match point with an uncertainty of only ± 0.6 pixels. This has been determined by repeat observations of the same image points, where the repetitions are spaced one day apart.

In a different radar sensor carried in an aircraft, the matching errors are slightly smaller due prob-

ably to a better signal-to-noise ratio, although the pixels are much smaller than in Magellan. However, when one studies SPOT images, one can conclude that the matching errors are at ± 0.7 pixels, both in rolling and in steeply mountainous terrains.

In digitized aerial photography the relevant discrepancies between an experienced operator and a machine-matching method amount to less than ± 0.5 pixel for smooth, and more than 2 pixels for extremely rugged terrain. Note the steep Flatirons rock formation of Boulder, Colorado which leads the matching algorithm to larger errors. One may expect that these errors would be reduced with an iterative orthorectification as proposed by Schenk et al. (1990) and demonstrated by Norvelle (1992b).

5.2. Accuracy variations as a function of matching methods

Fig. 11 plots the standard deviations between manual and automated matching as a function of the reference area ($M \times M$), using a fixed value of $N - M = 10$. The area used was Fig. 5 (rugged). We find the expected result, namely that the normalized correlation coefficient, r, produces the match points closest to the manual selection. This conclusion generally applies at all window sizes and all data sets. For the sake of brevity we do not report the extensive computations which verify the validity of this conclusion.

5.3. How many errors are larger than one pixel?

In Fig. 12 we present the percentage of observations that do not exceed a one pixel difference in both x and y between manual and automated matching for various window sizes. In all Magellan data we find that errors exceed 1 pixel at least 50% of the time. The accuracy increases to a maximum around a reference window size of 40.

The same presentation, when applied to different image types, leads to the conclusion that with SPOT, this percentage is $<10\%$ for ≥ 1 pixel; it is $<15\%$ in aerial photography. In mountainous and flat areas, the percentages differ with smaller errors in flat areas.

An operator examining the automated matches will want to correct this percentage of erroneous matches since the surface visibly deviates from that defined by machine.
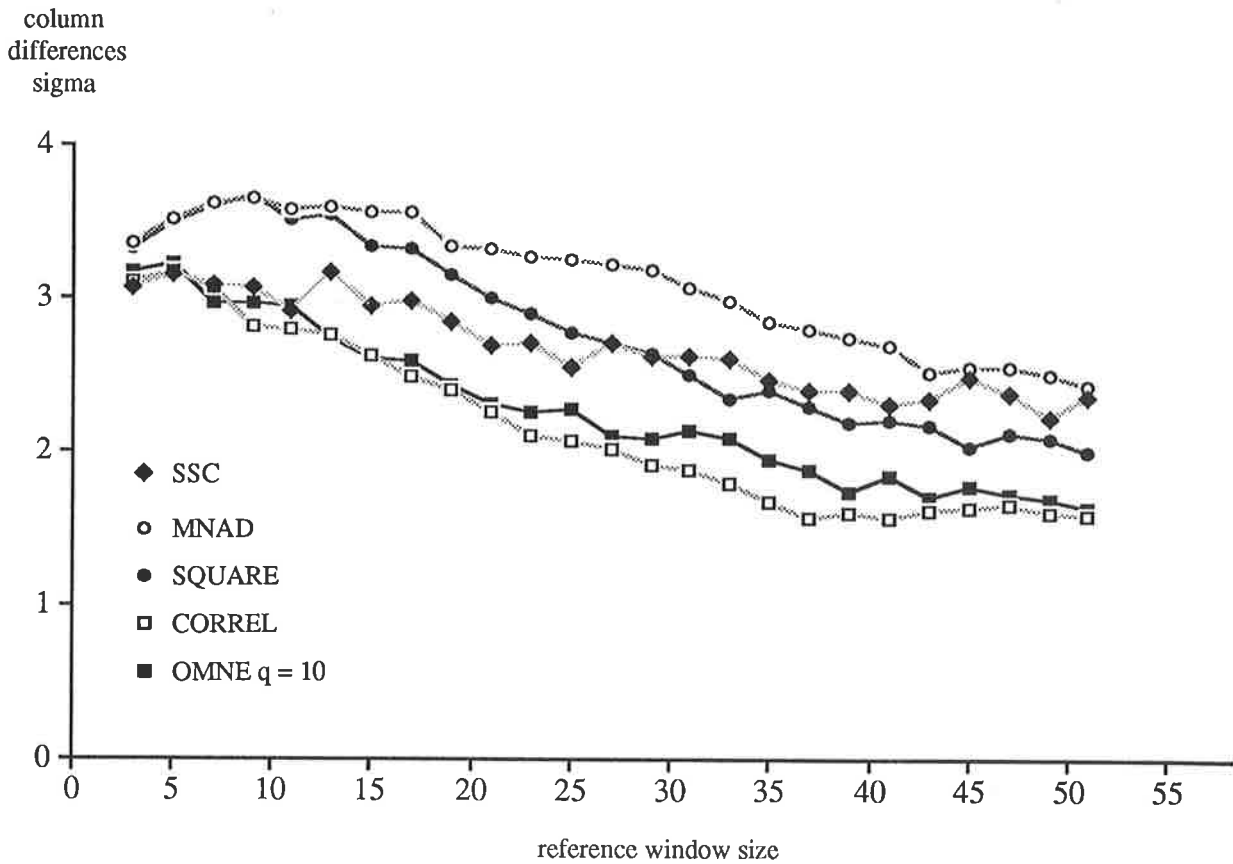
column
differences
sigma

Figure 11. Comparing matching methods by plotting $\sigma_{\Delta x}$ for each reference window size (M) of the match surface, for the stereo model in Figs. 5c and 5d (39°S).

5.4. The effect of inaccurate predictions

So far the Δx-values were reported as defined by the best available manual match points. If one modifies the manual match by several pixels, then the search window encompasses different pixels than previously used (see Fig. 10). As a result one may find a shift from the result of the automated matches.

In general the effect of falsifying the predictor is seen as being similar to increasing the size of the search window. We plan to study this effect (Figs. 11, 12) and hypothesize that the match performance again peaks around a window size of 40 at which point mismatches increase and performance begins to decline.

5.5. Illustrating digital elevation models from manual and automated matches

The pair of Magellan images from an area near that in Fig. 1 was subjected to the creation of a Digital Elevation Model (DEM) as described by Leberl et al. (1992). This implies that the match points be converted to stereo-parallaxes p or, preferably, to stereo-parallax differences Δp:

$$\Delta p_P = (x_P'' - x_P') - (x_A'' - x_A')$$

This means that one terrain point, A, is selected as a datum point and all other points, P, get their parallax defined with respect to A. The parallax differences, Δp, are then converted to terrain elevation differences, Δh, as follows:

$$\Delta h = \left(\frac{1}{\tan\theta'} - \frac{1}{\tan\theta''} \right) \times \Delta p$$
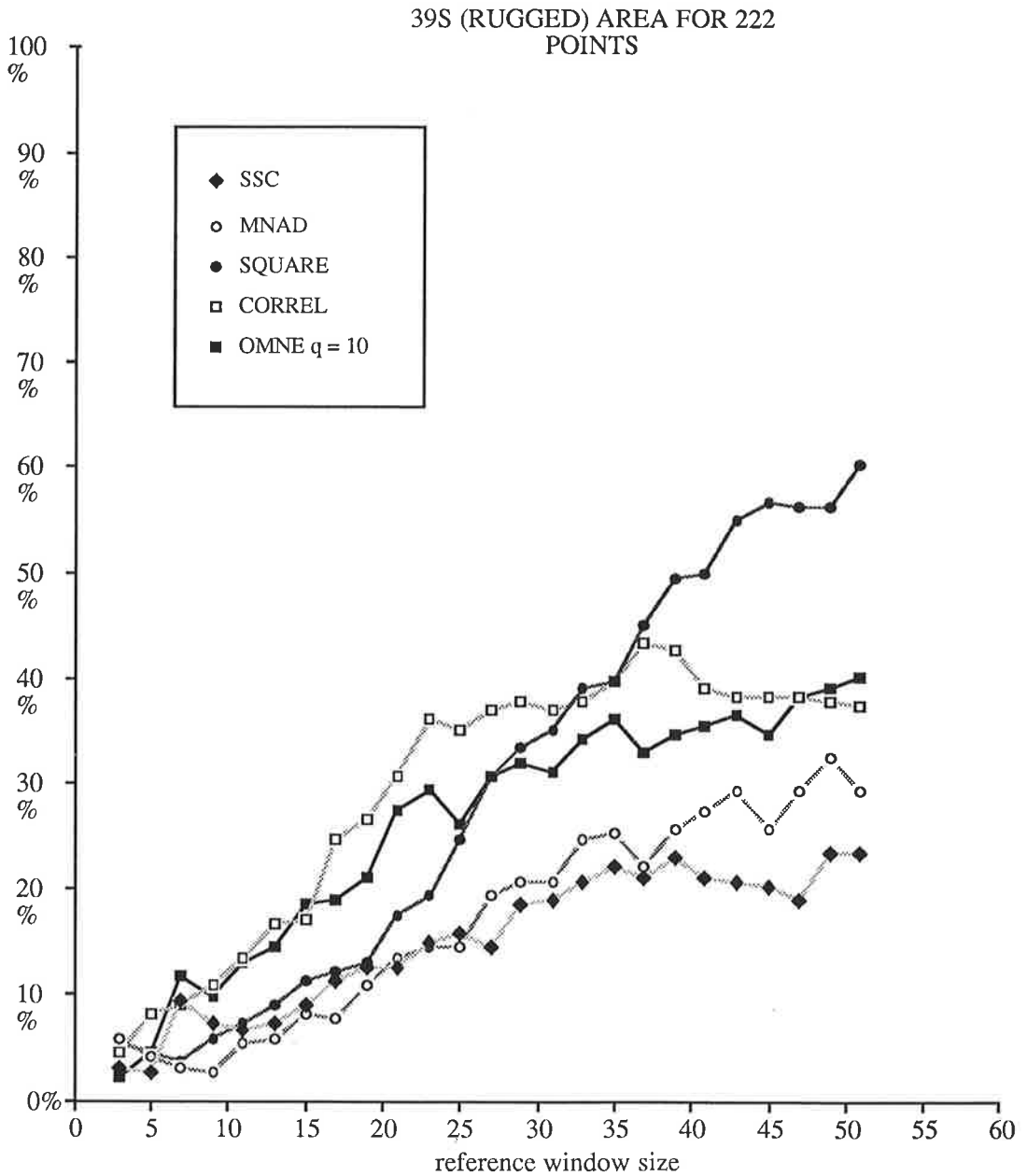
Figure 12. Percentage of match errors Δx which do not exceed one pixel from Fig. 5 (rugged).

with θ', θ'' being the look angles off-nadir of the Magellan images.

The individual Δh-values are associated with each of the x', y' observations in the left Magellan image. A DEM is now produced by shifting the x' coordinate by dx to correct the image position for the effect of the terrain elevation:

$$x = x' + dx = x' + h \tan \theta'$$

The resulting points at (x, y', h) are input to a gridding algorithm that creates a square-grid DEM and contour lines.

Applying this process to the images in Fig. 13, using both the manually found match points and the machine matches, results in the DEMs in Fig. 14 and the difference DEM in Fig. 15.

The automated matching process applied in the DEM is based on the normalized correlation
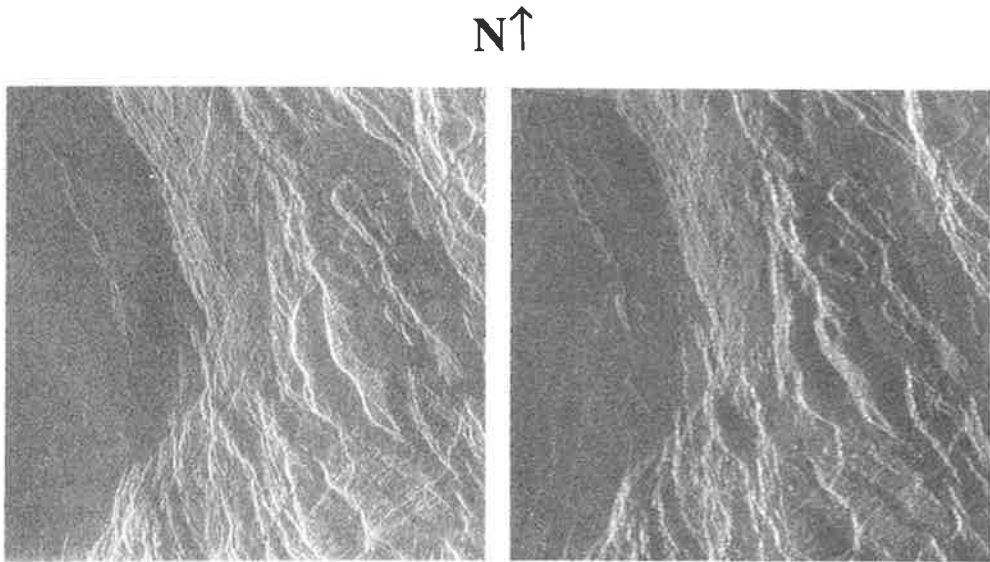
N↑

Figure 13. Image pair used to produce Figs. 14 and 15 (taken from the same areas as Fig. 1). The area is about 38×38 km^2.
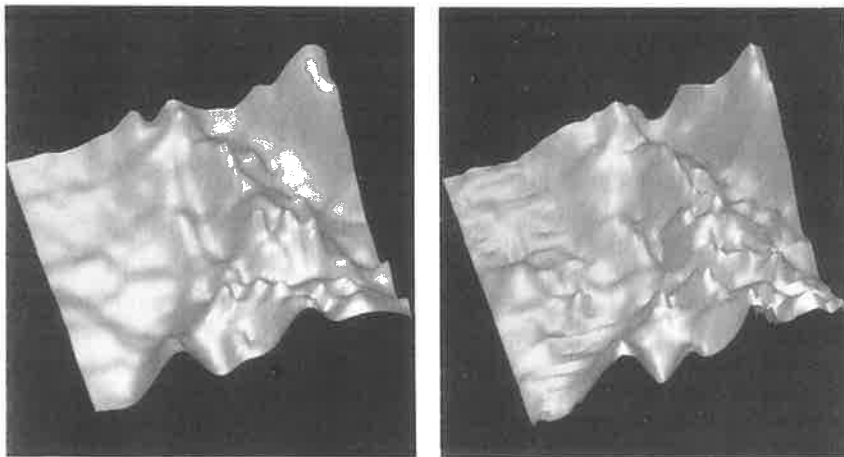

Figure 14. Digital elevation models produced by hand (left), and produced from automated machine matches (right), for the stereo model in Fig. 1. Differences have a standard deviation of 100 m. The terrain elevations from lowest to highest point are 2.6 km.

coefficient implemented within an algorithm that employs so-called "window-shaping" to improve the matching quality (Norvelle, 1992a). It should be noted that the automated method still requires manual acquisition of one row and one column of match points by an operator to kick-off the process.

The differences between manual and automated DEM creation are noisy with a standard deviation of $\sigma_h = \pm 100$ m. We also find a mean error dh_{mean} of measuring parallaxes which is not relevant in the current study since all coordinates are measured in local systems. The ± 100 m error is consistent with the expected ± 2 pixel parallax discrepancy between manual and machine-observed parallaxes: 2 pixels represent 150 m in parallax, converting to a ± 100 m height error. The automated matching process produces matching errors which result in elevations with a random elevation component. A low-pass filter can reduce this error and will eliminate the random error component. It cannot, however, produce the DEM at an accuracy equal to that obtained by an experienced stereo-operator.

Figure 15. Difference DEM produced by taking the absolute values of the differences in height at each point of the two DEMs in Fig. 14. The r.m.s. difference is ±100 m. Note the high frequency of the errors.

6. Conclusions and outlook

We have quantified the expected errors of machine matches in Magellan radar images. We applied conventional matching techniques that lend themselves to implementation in a massive global DEM-effort for planet Venus. We compared machine matches with those of an experienced photogrammetric stereo-operator. We have found these errors to be ±2 pixels, confirming accuracy statements reported in the literature (e.g. Simard et al., 1986). We have also shown that radar matching errors are larger than those in SPOT images or digitized aerial photography.

We can speculate that errors are larger due to radar speckle noise and the illumination differences inherent in stereo radar images, but absent in SPOT and aerial photography. We studied the size of matching errors as they depend on matching algorithms, on types of terrain and on the size of the window used to compute a match. The results are all expressed in terms of "pixels", thereby eliminating the issue of scale. However, for one example we produced a full DEM by hand and via automated matches. This illustrated the random character of the match errors and permitted one to quantify the DEM elevation differences (between manual and machine results) at ±100 m.

As one wishes to automate image matches, one needs to be aware of the limitations of matching

algorithms. Improvements can be attempted by accounting for the differences in the two images. An example is the use of the DEM to orthorectify the two input images and rematch them. If the DEM were error-free, then the two orthorectified images would match. Any mismatches can be used to refine the DEM.

One may argue that area-based matching ignores the "push-broom"-like geometry of kinematic SAR image sensing. This may indeed serve to reduce the computational effort in each match by searching for the match point along a line of constant azimuth. We do not expect, however, an increase in accuracy.

We assume that the major factors in defining matching accuracy are the geometric and radiometric differences among overlapping images. Therefore one may wish to devise an iterative matching strategy that accounts for geometric differences through geometric warping and radiometric differences by shape-from-shading.

One might also employ a matching model which includes the gray values as a function of terrain slope in a simultaneous adjustment. The study of the potential for improvement from such refinements must be the subject of future work.

References

Anuta, P., 1970. Spatial registration of multispectral and multitemporal digital imagery using fast Fourier transform techniques. IEEE Trans. Geosci. Electron., GE-8, October.

Crombie, M.A. and Bosch, E.H., 1986. An edge detection experiment using the MAR operator. Rep. ETL-0435, U.S. Army Corps of Engineers, Topographic Engineering Center, Fort Belvoir, Va., 20 pp.

Fernin, P. and Nasr, J.-M., 1990. Edge detection and Hough transform techniques applied to high-relief SAR imagery

for automated registration. Proc. IGARSS '90, College Park, Md. pp. 643–646.

Guindon, B., 1987. A combined shape-from-shading and feature matching technique for the acquisition of ground control points in SAR images of rugged terrain. Proc. ISPRS Symp. Comm. VII, Victoria, B.C., pp. 811–813.

Guindon, B. and Maruyama, H., 1986. Automated matching of real and simulated SAR imagery as a tool for ground control point acquisition. Can. J. Remote Sensing, 12 (4): 149–158.

Herbin, M., Venot, A. Devaux, J.Y., Walter, E., Lebruchec, J.F., Dubertret, L. and Roucayrol, J.C., 1989. Automated registration of dissimilar images: application to medical imagery. Comput. Vision, Graph. Image Process., 47 (1): 77–88.

Leberl, F.W., Maurice, K., Thomas, J. and Kober, W., 1991. Radargrammetric measurements from the initial Magellan coverage of planet Venus. Photogramm. Eng. Remote Sensing, 57 (12): 1561–1570.

Leberl, F.W., Thomas, J.K. and Maurice, K.E., 1992. Initial results from the Magellan stereo experiment. J. Geophys. Res., 97, E8: 13675–13689.

Li, M., 1991. Hierarchical multipoint matching. Photogramm. Eng. Remote Sensing, 57 (8): 1039–1047.

Norvelle, F.R., 1992a. Stereo correlation: window shaping and DEM corrections. Photogramm. Eng. Remote Sensing, 58 (1): 111–115.

Norvelle, F.R., 1992b. Using iterative orthophoto refinements to correct digital elevation models (DEM's). Proc. 1992 Am. Soc. Photogramm. Remote Sensing Annu. Mtg. Conv., Albuquerque, N.M., 1: 347–355.

Ramapriyan, H.K., Strong, J.P., Hung, Y. and Murray, C.W., 1986. Automated matching of pairs of SIR-B images for elevation mapping. IEEE Trans. Geosci. Remote Sensing, GE-24 (4): 462–472.

Rosenholm, D., 1987. Multi-point matching using the least-square technique for evaluation of three-dimensional models. Photogramm. Eng. Remote Sensing, 53 (6): 621–626.

Schenk, T., Li, L.C. and Toth, C.K., 1990. Iteratively rectified imagery. Proc. Int. Soc. Photogramm. Remote Sensing, Comm. V., Vol. 28, Part 5/1, pp. 464–470.

Schenk, T., Li, J.-C. and Toth, C., 1991. Towards an autonomous system for orienting digital stereopairs. Photogramm. Eng. Remote Sensing, 57 (8): 1057–1064.

Simard, R., Plourde, F. and Toutin, T., 1986. Digital elevation modelling with stereo SIR-B image data. Proc. ISPRS Comm. VII Symp. Remote Sensing for Resources Development and Environmental Management, ITC, Enschede, pp. 161–166.

Svedlow, M., McGillem, C.D. and Anuta, P.E., 1978. Image registration: similarity measure and preprocessing method comparisons. IEEE Trans. Aerosp. Electron. Syst., AES-14 (1): 141–149.